

Human Following for Wheeled Robot with Monocular Pan-tilt Camera

Zheng Zhu, Hongxuan Ma, Wei Zou

Abstract—Human following on mobile robots has witnessed significant advances due to its potentials for real-world applications. Currently most human following systems are equipped with depth sensors to obtain distance information between human and robot, which suffer from the perception requirements and noises. In this paper, we design a wheeled mobile robot system with monocular pan-tilt camera to follow human, which can stay the target in the field of view and keep following simultaneously. The system consists of fast human detector, real-time and accurate visual tracker, and unified controller for mobile robot and pan-tilt camera. In visual tracking algorithm, both Siamese networks and optical flow information are exploited to locate and regress human simultaneously. In order to perform following with a monocular camera, the constraint of human height is introduced to design the controller. In experiments, human following are conducted and analysed in simulations and a real robot platform, which demonstrate the effectiveness and robustness of the overall system.

I. INTRODUCTION

Tracking and following human on mobile robots within cameras are of significance for human-computer interaction [1], [2], automatic driving [3], [4], personal assistant robot [5], [6], [7] and service robot [8], [9], [10], [11], [12]. The core technology for the following robot mainly consists of human visual tracker and robot controller. The former tracks a specified human in a changing video sequences automatically given a detected bounding box in the first frame, while the controller generates necessary motion commands so that the robot can follow the target human.

The core problem of visual tracking is how to detect and locate the object accurately and fast in human following scenarios with occlusions, shape deformation, illumination variations [13], [14], [15], [16], [17], [18]. Similarly with other computer vision tasks [19], [20], [21], [22], [23], [24], [25], [26], [27], [28], [29], [30], deep convolutional networks have achieved favourable performance in recent tracking benchmarks [31], [32], [33], [34], [35], [36], [37], [38], [39], [40], [41], [42], [43], [44], [45], [46], [47], [48], [49]. In this paper, both Siamese networks [47], [48] and optical flow information [44], [50], [51] are exploited to locate and regress human simultaneously. Besides, negative pairs of human are emphasised to suppress the response of distractor. A simple yet effective failure recovery strategy is proposed to handle the occlusion and out-of-view during tracking.

Since distance information of target is essential for robot perception and control, depth sensors are always equipped for following task [52], [53], [54], [55], [56], [57], [58],

[59]. Laser scans with camera are always used to detect and track the fixed height legs of human [59], which cannot provide robust features for discriminating the different persons following task. Kinect cameras are frequently adopted in the robotics community [53], [55], [57], whose minimum distance requirement and sensitivity to the illumination variations limit its applications. Some robots [56] are equipped with stereo vision systems to reconstruct the depth information, which suffer from baseline configuration, camera calibration and field of view problems. In paper [60], monocular camera with an ultrasonic sensor are adopted to implement the human tracking system. However, the accuracy of ultrasonic sensor is always effected by reflection problem and noise. Above sensors are fixed to the robots, which limits the range of perception. In this paper, we develop a wheeled mobile robot system with monocular pan-tilt camera, which does not need the distance information provided by depth sensors. Besides, The camera can actively track human using pan-tilt motors. In order to perform following with a monocular camera, the constraint of human height is introduced to design unified controller for wheeled robot and pan-tilt camera.

The rest of this paper is organized as follows: Section II describes our designed human following systems, including robot configuration, fast human detector, real-time and accurate visual tracker, and unified controller for mobile robot within pan-tilt camera. Section III shows experiment results on human following scenarios. Section IV concludes the paper with a summary.

II. FOLLOWING HUMAN UTILIZING MOBILE ROBOT WITHIN MONOCULAR PAN-TILT CAMERA

In this section, we introduce the overall framework of human following system at first. Then the separate parts, including robot system and coordinate definition, fast human detector, real-time and accurate visual tracker, and unified controller for mobile robot within pan-tilt camera are detailed described respectively.

A. Overall Human Following Framework

The overall human following framework consists of human detection and tracking in captured video streaming and controller for mobile robot within pan-tilt camera. At the beginning of human following, the human bounding box is indicated by tiny YOLO [61] detector. Once the initial box is given, human tracking loop is performed using the proposed *FlowTrack++* algorithm. Tracking results are fed into the controller for mobile robot and pan-tilt platform, which results in the motion of camera. Both the visual tracker

and robot controller form a closed loop for human following task as shown in Figure 1.

B. Robot System and Coordinate Definition

As shown in Figure 2, a wheeled mobile robot within monocular pan-tilt camera is adopted in this paper to achieve human following task. The robot system consists of a wheeled mobile platform and a pan-tilt camera platform. The wheeled mobile platform are equipped with a microcomputer (including a GTX1050Ti GPU). The pan-tilt camera platform contains pan/tilt motors as well as their corresponding encoders. Compared with conventional human tracking systems that are equipped with fixed depth sensors, our hardware structure has a larger field-of-view and are less suffered from the perception requirements as well as noises.

Right part of Figure 2 illustrates the coordinate systems used in this paper. $F_r = (O_r : X_r, Y_r, Z_r)$ represents the mobile robot coordinate system whose origin locates at the midpoint of two wheels axis, and the X_r -axis is aligned with the forward direction of mobile robot. $F_a = (O_a : X_a, Y_a, Z_a)$ and $F_b = (O_b : X_b, Y_b, Z_b)$ are defined as pan and tilt coordinate systems respectively. $F_c = (O_c : X_c, Y_c, Z_c)$ is the camera coordinate system. At the beginning, the X_a -axis is aligned with Y_r -axis and Y_a -axis is aligned with Z_r -axis. The origin of F_a is the same with F_r , and the origin of F_c is the same with F_b . The direction of Z_a -axis changes as the pan motor rotates α , and the direction of Z_c -axis changes as the tilt motor rotates β . All axis of F_a are always aligned with the corresponding axis of F_b .

C. Fast Human Detector

YOLO [61] is utilized as detector in human following task because of its superior speed and accuracy. In this framework, single neural network predicts bounding boxes and class probabilities directly from full images, which regards object detection as a regression problem. Specifically, YOLO divides the full image into 7×7 grid and for each grid cell predicts 2 bounding boxes, confidence for those boxes, and their class probabilities. For our following task, only *person* class is adopted while other classes are ignored. We implement Tiny YOLO version on the mobile robot platform where it can perform at 80 FPS. The human bounding box is initialized when the detected position is less than 10 pixels among three consecutive frames.

D. Real-time and Accurate Visual Tracker

In this subsection, the overall architecture of proposed *FlowTrack++* algorithm is introduced, which gracefully combines flow aggregation module [44] and high-quality Siamese network [47], [48]. As shown in Figure 3, the Siamese network contains a kernel branch and a search branch. In kernel branch, the feature maps of template frame is extracted by FeatureNet. In search branch, the flow aggregation module contains FeatureNet (feature extraction sub-network), FlowNet [62], warping module, attention-guided fusion module. Appearance features and flow information are

extracted by the FeatureNet and FlowNet at first. Then previous frames at predefined intervals is warped to t frame guided by flow information. Meanwhile, a attention-guided fusion module is designed to weight the warped feature maps. More details about flow aggregation module can be found in [44]. Finally, both two branches are fed into subsequent high-quality Siamese network for simultaneous classification and regression [47]. All the modules are differentiable and trained end-to-end.

There are always other person and object in the human following scenarios, which may drift the tracking results. Besides, conventional visual tracking algorithms lack consideration for occlusion and out-of-view, which occur frequently in human following. To address these problems, inspired by [48], we adopt hard-negative samples mining strategy and failure recovering strategy.

a) *Hard-negative Samples Mining*: The hard-negative samples contains intra-class pairs and inter-class pairs. In implementations, intra-class pairs are sampled from the different videos that is labelled as *person* (i.e different person from different video). Similarly, inter-class pairs are sampled from the different videos that is labelled different class, such as person and car from different video. All the image pairs are sent to two branches of Figure 3 to train the FlowTrack++ algorithm. After the hard-negative samples are addressed in training process, the results map of Siamese network becomes high-quality: the high response only appear in the desired target, where the responses of other position (including other human and objects) is suppressed due to the proposed training strategy.

b) *Failure Recovering*: Human following task always encounters occlusion and out-of-view because of the unconstrained environments and drastic camera motions. Conventional trackers lack handling mechanism towards these challenges, which may cause permanent tracking failure. In this paper, a simple yet efficient failure recovering strategy is designed based the high-quality Siamese network output. Specifically, When the failed tracking is indicated (highest score of results map is lower than the threshold), the size of search region is iteratively increased with a constant step size s until the target is re-detected. This module significantly improves the performance in out-of-view and occlusion challenges. The iterative local-to-global search strategy does not cover the entire images in most cases. This is more efficient than that version of SINT [63] which samples over the whole image and adopts time-consuming multi-scale test strategy. The proposed FlowTrack++ algorithm can perform at 40 FPS in human following scenarios. The detailed process of our failure recovering strategy is described in Algorithm 1.

E. Unified Controller

In this paper, the controller is designed to stay the human bounding box near the center of view and keep the half height h of the tracking box near a pre-defined constant H , which is illustrated in Figure 4. The visual servo formulation is adopted to derive our controller:

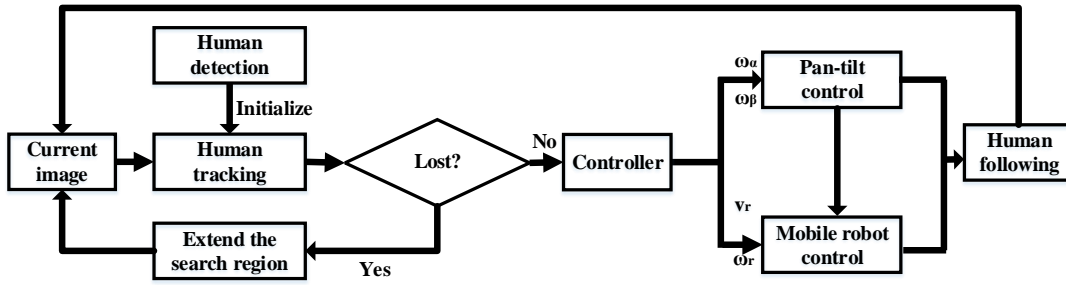


Fig. 1: The overall framework for human following.

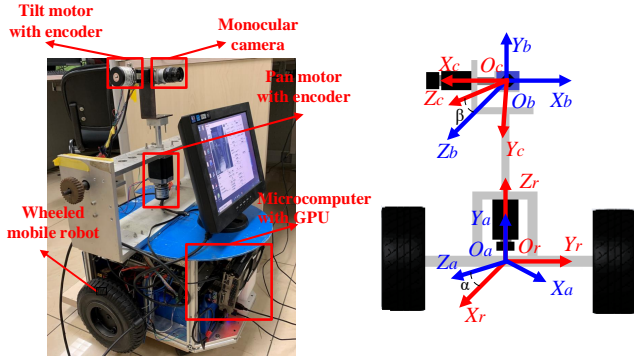


Fig. 2: Left part is the designed robot platform for human following task. Right part is corresponding coordinate systems.

Algorithm 1 Algorithm for recovering from tracking failure

Require: thresholds Th_{low} and Th_{high} to enter and quit failure cases.

Ensure: target position P_t and tracking score S_t during sequences.

- 1: set $failure_state = False$
 - 2: perform normal tracking in the first frame, get the position P_t and the score S_t .
 - 3: **repeat**
 - 4: **if** $S_t \leq Th_{low}$ **then**
 - 5: set $failure_state = True$
 - 6: **else**
 - 7: **if** $S_t \geq Th_{high}$ **then**
 - 8: Set $failure_state = False$
 - 9: **end if**
 - 10: **end if**
 - 11: **if** $failure_state$ **then**
 - 12: increase the search region by the iterative local-to-global strategy, perform tracking with this larger region, get the position P_t and the score S_t .
 - 13: **else**
 - 14: perform normal tracking, get the position P_t and the score S_t .
 - 15: **end if**
 - 16: **until** end of video sequences.
-

$${}^c\dot{P}_t = -{}^c v_c - {}^c \omega_c \times {}^c P_t \quad (1)$$

where ${}^c P_t$ is the human target coordinate in camera coordinate system, ${}^c v_c$ and ${}^c \omega_c$ are the linear and angular velocity of the camera in the camera coordinate, respectively. ${}^c v_c$ and ${}^c \omega_c$ can be obtained as follows:

$${}^c v_c = {}^c R_r {}^r v_c = {}^c R_r \begin{bmatrix} V_r \\ 0 \\ 0 \end{bmatrix} \quad (2)$$

$${}^c \omega_c = {}^c R_r \begin{bmatrix} 0 \\ 0 \\ \omega_r + \omega_\alpha \end{bmatrix} + \begin{bmatrix} \omega_\beta \\ 0 \\ 0 \end{bmatrix} \quad (3)$$

where ${}^c R_r$ denotes the rotation matrix from F_r to F_c , V_r is the velocity of the mobile robot, ω_α and ω_β denote the the pan and tilt angular velocity of the camera respectively, and ω_r represents the robot angular velocity.

Substituting (2) and (3) into (1), equation (1) can be rewritten as follows:

$$\begin{bmatrix} \dot{c}x \\ \dot{c}y \\ \dot{c}z \end{bmatrix} = \begin{bmatrix} -V_r \sin \alpha + (\omega_\alpha + \omega_r) \cos \beta^c z - (\omega_\alpha + \omega_r) \sin \beta^c y \\ V_r \cos \alpha \sin \beta + (\omega_\alpha + \omega_r) \sin \beta^c x - \omega_\beta^c z \\ -V_r \cos \alpha \cos \beta + \omega_\beta^c y - (\omega_\alpha + \omega_r) \cos \beta^c x \end{bmatrix} \quad (4)$$

The control objective is to stay the human bounding box near the center of view and keep the half height h of box near a pre-defined constant H . To this end, the three image errors in pixel level are defined as:

$$\begin{cases} e_u = u - u_0 \\ e_v = v - v_0 \\ e_{v2} = v - v_2 - H \end{cases} \quad (5)$$

where (u, v) is the center point of human bounding box, (u, v_2) is the middle point of top border, (u_0, v_0) is the center point of captured image, H is a pre-defined constant, which is the half of the desired height of tracking box. The relationship between coordinate systems F_b and F_c is:

$$\begin{bmatrix} b_x \\ b_y \\ b_z \\ 1 \end{bmatrix} = \begin{bmatrix} 1 & 0 & 0 & 0 \\ 0 & \cos \beta & -\sin \beta & 0 \\ 0 & \sin \beta & \cos \beta & 0 \\ 0 & 0 & 0 & 1 \end{bmatrix} \begin{bmatrix} c_x \\ c_y \\ c_z \\ 1 \end{bmatrix} \quad (6)$$

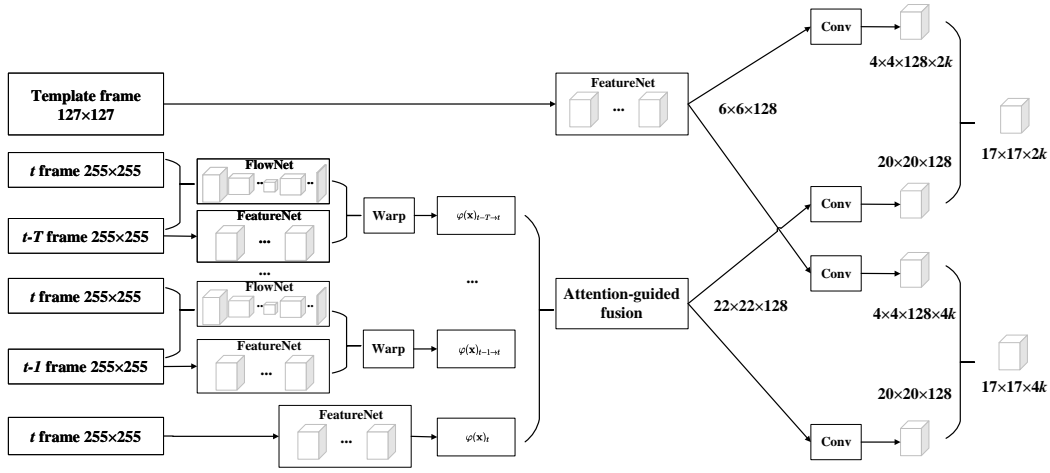


Fig. 3: The overall framework for FlowTrack++ algorithm. The input size of kernel branch (top) and search branch (bottom) are 127×127 and 255×255 , respectively. The output size of FeatureNet in kernel branch is $6 \times 6 \times 128$, which is transformed to a $4 \times 4 \times 128 \times 2k$ kernel and a $4 \times 4 \times 128 \times 4k$ kernel (k is the anchor number in each position) by two 3×3 convolution layers. Similarly, the output size of attention-guided fusion in search branch is $22 \times 22 \times 128$, which is extended to two $20 \times 20 \times 128$ feature maps by 3×3 convolution layer. Finally, the feature map and kernels are correlated to produce $17 \times 17 \times 2k$ classification map and $17 \times 17 \times 4k$ regression map.

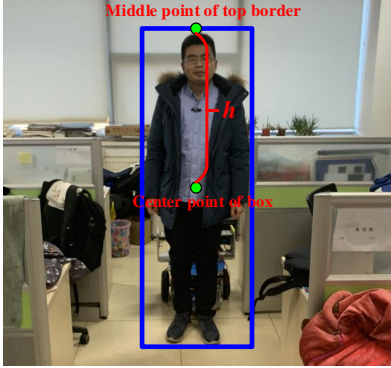


Fig. 4: The control objective is to stay the human bounding box near the center of view and keep the half height of box (h) near a pre-defined constant H .

Since human and mobile robot move on the flat ground, we can assume that the height of human in coordinate system F_b , i.e. ${}^b y$ remains constant. According to equation (5), (6) and pin-hole camera model ($\alpha_x, \alpha_y, u_0, v_0$ are camera intrinsic parameters, $({}^c x, {}^c y, {}^c z)$ represents a point in camera coordinate system and (u, v) is its corresponding image coordinate), the relationship between ${}^c z$ and ${}^b y$ can be obtained:

$${}^c z = \frac{\alpha_y \cdot {}^b y}{e_v \cos \beta - \alpha_y \sin \beta} \quad (7)$$

(7) into consideration, we can obtain equation (8).

$$\begin{cases} \dot{e}_u = \lambda_1 V_r \Omega_1 + A(\omega_\alpha + \omega_r) + B\omega_\beta \\ \dot{e}_v = \lambda_1 V_r \Omega_2 + C(\omega_\alpha + \omega_r) + D\omega_\beta \\ \dot{e}_{v2} = \lambda_1 V_r \Omega_2 + C(\omega_\alpha + \omega_r) + D\omega_\beta - \lambda_2 V_r \Omega_3 \\ - E(\omega_\alpha + \omega_r) - F\omega_\beta \end{cases} \quad (8)$$

where $\lambda_1 = \frac{1}{v_{y1}}$ and $\lambda_2 = \frac{1}{b_{y2}}$, ${}^b y_1$ is the y-coordinate of the center point of human body, and ${}^b y_2$ is the y-coordinate of the middle point of top border as shown in Figure 4. They are both donated in coordinate system F_b . The meaning of other symbols are shown in equation (9).

$$\begin{cases} \Omega_1 = \frac{1}{\alpha_y} (\alpha_x \sin \alpha - e_v \cos \alpha \cos \beta) (e_v \cos \beta + \alpha_y \sin \beta) \\ \Omega_2 = \frac{1}{\alpha_y} (e_v \cos \alpha \cos \beta + \alpha_y \cos \alpha \sin \beta) \cdot \\ (-e_v \cos \beta - \alpha_y \sin \beta) \\ \Omega_3 = \frac{1}{\alpha_y} ((v_2 - v_0) \cos \alpha \cos \beta + \alpha_y \cos \alpha \sin \beta) \\ (-v_2 - v_0) \cos \beta - \alpha_y \sin \beta \\ A = \frac{1}{\alpha_x \alpha_y} (\alpha_x^2 \alpha_y \cos \beta - \alpha_x^2 \sin \beta e_v + e_u^2 \alpha_y \cos \beta) \\ B = -\frac{1}{\alpha_y} (e_u e_v) \\ C = \frac{1}{\alpha_x} (\alpha_y \sin \beta e_u + e_u e_v \cos \beta) \\ D = -\frac{1}{\alpha_y} (\alpha_y^2 + e_v^2) \\ E = \frac{1}{\alpha_x} (\alpha_y \sin \beta (u_2 - u_0) - (u_2 - u_0)(v_2 - v_0) \cos \beta) \\ F = -\frac{1}{\alpha_y} (\alpha_y^2 + e_{v2}^2) \end{cases} \quad (9)$$

Differentiating equation (5) to time on both sides and take

$$V_r = -\frac{(BC - AD)(K_2 e_v - K_3 e_{v2}) + (AF - BE)K_2 e_v - (CF - DE)K_1 e_u}{(BC - AD)\Omega_3 \lambda_2 + (AF - BE)\Omega_2 \lambda_1 - (CF - DE)\Omega_1 \lambda_1} \quad (13)$$

$$\omega_\alpha = \frac{(DK_1 e_u - BK_2 e_v - BC\omega_r + AD\omega_r)\Omega_3 \lambda_2 + (BE\omega_r - AF\omega_r - BK_3 e_{v2} + BK_2 e_v - FK_1 e_u)\Omega_2 \lambda_1 + (CF\omega_r - DE\omega_r + DK_3 e_{v2} - DK_2 e_v + FK_2 e_v)\Omega_1 \lambda_1}{(BC - AD)\Omega_3 \lambda_2 + (AF - BE)\Omega_2 \lambda_1 - (CF - DE)\Omega_1 \lambda_1} \quad (14)$$

$$\omega_\beta = \frac{(CK_3 e_{v2} - CK_2 e_v + EK_2 e_v)\Omega_1 \lambda_1 - (AK_2 e_v \lambda_2 - CK_1 e_u)\Omega_3 \lambda_2 - (AK_2 e_v + AK_3 e_{v2} + EK_1 e_u)\Omega_2 \lambda_1}{(BC - AD)\Omega_3 \lambda_2 + (AF - BE)\Omega_2 \lambda_1 - (CF - DE)\Omega_1 \lambda_1} \quad (15)$$

$$\omega_r = \begin{cases} 0, & -\frac{\pi}{6} < \alpha < \frac{\pi}{6} \\ 0.1\alpha, & \alpha < -\frac{\pi}{6} \text{ or } \alpha > \frac{\pi}{6} \end{cases} \quad (16)$$

To make errors converge to zero, the following equations should be satisfied:

$$\begin{cases} \dot{e}_u = -K_1 e_u \\ \dot{e}_v = -K_2 e_v \\ \dot{e}_{v2} = -K_3 e_{v2} \end{cases} \quad (10)$$

where K_1 , K_2 and K_3 are positive gains respectively. Substituting (8) and (9) into (10), robot linear velocity, pan and tilt angular velocity of the camera can be obtained by equations (13), (14), and (15) respectively. Besides, the strategy to control the robot angular velocity ω_r is adopted as equation (16).

III. EXPERIMENTS

A. Simulation Results of Control Law

In this section, simulations are performed to verify the effectiveness of proposed controller. A rectangle is utilized to simulate the tracked human, where the control objective is to stay the human bounding box near the center of view and keep the half height of box near a pre-defined constant H . In our simulation, the human moves along a circle in world coordinate system. The center of the circle is at $(0.5, 0.5)$, and it is denoted as the following equation:

$$\begin{cases} x_t = 0.5 - 0.4 \cos(t) \\ y_t = 0.5 - 0.4 \sin(t) \end{cases} \quad (17)$$

The robot starts moving from $(0, 0)$ in the world coordinate system and H is set to 100. As shown in Figure 5 the proposed controller results in a smooth trajectory. Because the object is moving along an circle, the ω_α changes in a sinusoidal wave. The height of the human in image changes little, so the ω_β changes a little. As the human moves, in order to adjust the size of rectangle in the image, the mobile robot moves forward and backward, and the value of V_r fluctuates slightly around 0. Due to motion of the human, e_u , e_v and e_{v2} are always changing. Besides, h can stay around 100 according to the designed controller. From above results, one can find that the control law is effective.

B. Human Following Results

In this section, the effectiveness of human following system is verified by indoor and outdoor experiments on real-world robot platform. The indoor experiment is conducted in our laboratory and the outdoor experiment is performed

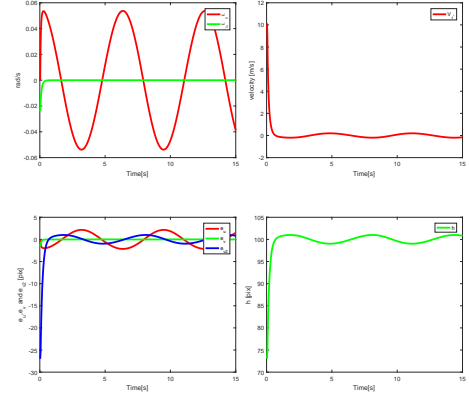


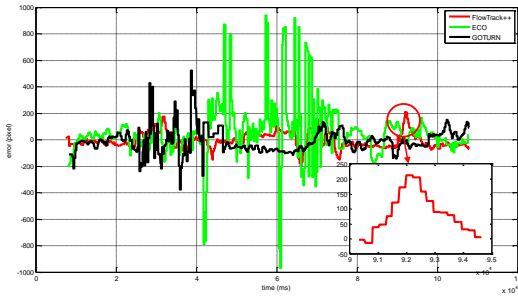
Fig. 5: The simulation result when the target moves along a circle, including the curves of ω_α and ω_β , the curve of V_r , the curves of e_u , e_v and e_{v2} , the curve of h .

outside the building in the Institute of Automation, Chinese Academy of Sciences. The height of the mounted camera is 0.7m, and the height of the person is about 1.8m. So the λ_1 and λ_2 in equation (8) are 5 and 0.91, respectively. We compared three different tracking algorithms on our designed controller, including proposed FlowTrack++, ECO [43] and GOTURN [64].

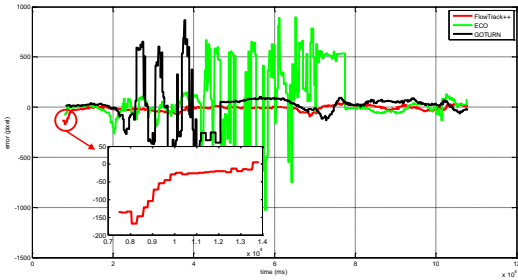
In indoors experiments, H is set as 500 pixel. Figure 6 shows the influence of different tracking algorithm on the controller. When adopting proposed FlowTrack++, the e_u increases to 211 pixels due to the relative motion between humans and robots while $t = 92s$. Then when $t = 95s$, e_u decreases to 0 quickly. Besides, the tracked human height h can stay around 500 pixels while other trackers fluctuate violently. From those results, it can be known that the tracking algorithms of FlowTrack++ have better performance on human following task.

In the outdoor experiments as shown in Figure 7, H is set as 300 pixel. By FlowTrack++ tracking algorithm, e_u and e_v can be kept around 0, and the h fluctuates stably around 300 pixels. Compared with FlowTrack++ algorithm, both ECO and GOTURN trackers result in larger tracking errors and unstable following results.

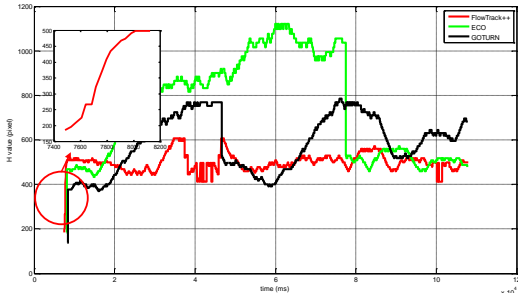
Figure 8 and Figure 9 further visualize the tracking results in human following task. Due to flow aggregation and box regression modules, FlowTrack++ can handle the pose changes and scale challenges in Figure 8. In Figure 9, targets are under occlusion, distractor and background changes. Since hard-negative samples mining and failure



(a)



(b)



(c)

Fig. 6: The results of indoor experiments. (a) Curves of e_u . (b) Curves of e_v . (c) Curves of h .

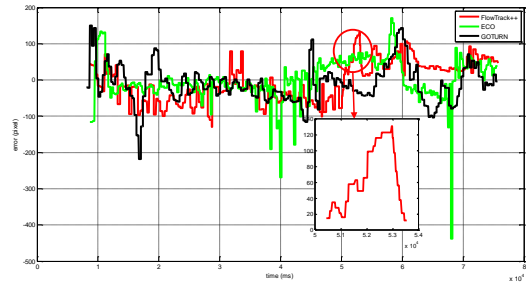
recovering strategies are adopted in FlowTrack++ algorithm, these challenges can be handled.

IV. CONCLUSION

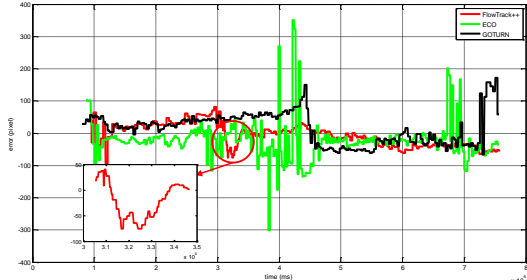
In this paper, we propose a human following system on mobile robot with monocular pan-tilt camera, which mainly consists of a visual tracker and a motion controller. In visual tracking algorithm, both Siamese networks and optical flow information are exploited to locate and regress human simultaneously. Besides, a motion controller is derived to stay the target in the field of view and keep following simultaneously, which does not need the depth sensors. In experiments, the overall system obtains accurate and robust following results both in simulations and real robot platform. Future work will explore the multi-object tracking and re-identification for human following task.

REFERENCES

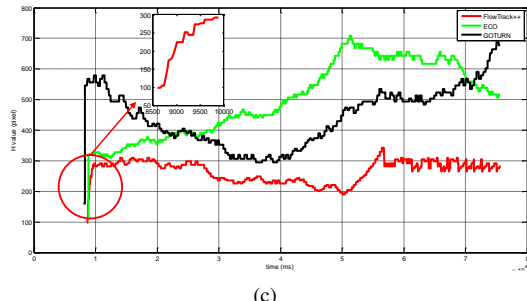
- [1] W. Luo, P. Sun, F. Zhong, W. Liu, T. Zhang, and Y. Wang, "End-to-end active object tracking and its real-world deployment via reinforcement learning," *IEEE Transactions on Pattern Analysis and Machine Intelligence*, 2019.



(a)



(b)



(c)

Fig. 7: The results of outdoor experiments. (a) Curves of e_u . (b) Curves of e_v . (c) Curves of h .

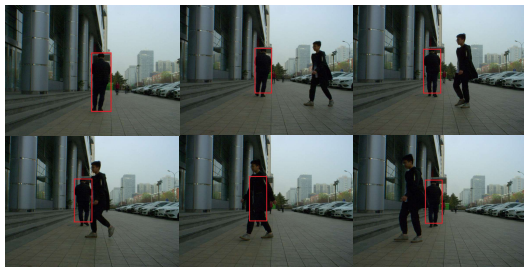


(a)



(b)

Fig. 8: Human tracking results in indoor experiments. (a) Pose changes challenge. (b) Scale challenge.



(a)



(b)

Fig. 9: Human tracking results in outdoor experiments. (a) Occlusion and distractor challenge. (b) Background changes challenge.

- [2] Q. Wang, W. Zou, D. Xu, and Z. Zhu, "Motion control in saccade and smooth pursuit for bionic eye based on three-dimensional coordinates," *Journal of Bionic Engineering*, vol. 14, no. 2, pp. 336–347, 2017.
- [3] S. Verma, Y. H. Eng, H. X. Kong, H. Andersen, M. Meghjani, W. K. Leong, X. Shen, C. Zhang, M. H. Ang, and D. Rus, "Vehicle detection, tracking and behavior analysis in urban driving environments using road context," in *2018 IEEE International Conference on Robotics and Automation*. IEEE, 2018, pp. 1413–1420.
- [4] A. Buyval, A. Gabdullin, R. Mustafin, and I. Shimchik, "Realtime vehicle and pedestrian tracking for didi udacity self-driving car challenge," in *2018 IEEE International Conference on Robotics and Automation*. IEEE, 2018, pp. 2064–2069.
- [5] N. Hirose, R. Tajima, and K. Sukigara, "Personal robot assisting transportation to support active human lifehuman-following method based on model predictive control for adjacency without collision," in *IEEE International Conference on Mechatronics*. IEEE, 2015, pp. 76–81.
- [6] R. Zhang, Z. Zhu, P. Li, R. Wu, C. Guo, G. Huang, and H. Xia, "Exploiting offset-guided network for pose estimation and tracking," in *Proceedings of the IEEE Conference on Computer Vision and Pattern Recognition Workshops*, 2019.
- [7] P. Li, J. Zhang, Z. Zhu, Y. Li, L. Jiang, and G. Huang, "State-aware re-identification feature for multi-target multi-camera tracking," in *Proceedings of the IEEE Conference on Computer Vision and Pattern Recognition Workshops*, 2019.
- [8] A. Bajcsy, S. L. Herbert, D. Fridovich-Keil, J. F. Fisac, S. Deglurkar, A. D. Dragan, and C. J. Tomlin, "A scalable framework for real-time multi-robot, multi-human collision avoidance," in *2019 International Conference on Robotics and Automation*. IEEE, 2019, pp. 936–943.
- [9] N. Bellotto and H. Hu, "Multisensor-based human detection and tracking for mobile service robots," *IEEE Transactions on Systems, Man, and Cybernetics, Part B (Cybernetics)*, vol. 39, no. 1, pp. 167–181, 2009.
- [10] N. Yao, E. Anaya, Q. Tao, S. Cho, H. Zheng, and F. Zhang, "Monocular vision-based human following on miniature robotic blimp," in *IEEE International Conference on Robotics and Automation*. IEEE, 2017, pp. 3244–3249.
- [11] H.-X. Ma, W. Zou, Z. Zhu, C. Zhang, and Z.-B. Kang, "Selection of observation position and orientation in visual servoing with eye-in-vehicle configuration for manipulator," *International Journal of Automation and Computing*, pp. 1–14.
- [12] Z. Kang, W. Zou, H. Ma, and Z. Zhu, "Adaptive trajectory tracking of wheeled mobile robots based on a fish-eye camera," *International Journal of Control, Automation and Systems*, vol. 17, no. 9, pp. 2297–2309, 2019.
- [13] P. Liang, Y. Wu, H. Lu, L. Wang, C. Liao, and H. Ling, "Planar object tracking in the wild: A benchmark," in *2018 IEEE International Conference on Robotics and Automation*. IEEE, 2018, pp. 651–658.
- [14] Y. Wu, J. Lim, and M. H. Yang, "Online object tracking: A benchmark," in *Proceedings of the IEEE Conference on Computer Vision and Pattern Recognition*, 2013, pp. 2411–2418.
- [15] L. Dressel and M. J. Kochenderfer, "Hunting drones with other drones: Tracking a moving radio target," in *2019 International Conference on Robotics and Automation*. IEEE, 2019, pp. 1905–1912.
- [16] Y. Wu and J. Lim, "Object tracking benchmark," *IEEE Transactions on Pattern Analysis and Machine Intelligence*, vol. 37, no. 9, pp. 1834–1848, 2015.
- [17] M. Kristan, A. Leonardis, J. Matas, M. Felsberg, R. Pflugfelder, L. Čehovin Zajc, T. Vojir, G. Hager, A. Lukežič, A. Eldesokey, and G. Fernandez, "The visual object tracking vot2017 challenge results," in *Proceedings of the The IEEE International Conference on Computer Vision Workshop*, Oct 2017.
- [18] M. Kristan, A. Leonardis, J. Matas, M. Felsberg, R. Pflugfelder, L. Č. Zajc, T. Vojir, G. Bhat, A. Lukežič, A. Eldesokey et al., "The sixth visual object tracking vot2018 challenge results," in *European Conference on Computer Vision*. Springer, Cham, 2018, pp. 3–53.
- [19] A. Krizhevsky, I. Sutskever, and G. E. Hinton, "Imagenet classification with deep convolutional neural networks," in *Proceedings of the Advances in Neural Information Processing Systems*, 2012, pp. 1097–1105.
- [20] K. He, X. Zhang, S. Ren, and J. Sun, "Deep residual learning for image recognition," in *Proceedings of the IEEE Conference on Computer Vision and Pattern Recognition*, 2016, pp. 770–778.
- [21] Y. Li, X. Chen, Z. Zhu, L. Xie, G. Huang, D. Du, and X. Wang, "Attention-guided unified network for panoptic segmentation," in *Proceedings of the IEEE Conference on Computer Vision and Pattern Recognition*, 2019, pp. 7026–7035.
- [22] T. Y. Lin, P. Dollr, R. Girshick, K. He, B. Hariharan, and S. Belongie, "Feature pyramid networks for object detection," in *Proceedings of the IEEE Conference on Computer Vision and Pattern Recognition*, 2017.
- [23] J. Zhang, Z. Zhu, W. Zou, P. Li, Y. Li, H. Su, and G. Huang, "Fastpose: Towards real-time pose estimation and tracking via scale-normalized multi-task networks," *arXiv preprint arXiv:1908.05593*, 2019.
- [24] J. Zhu, Z. Zhu, and W. Zou, "End-to-end video-level representation learning for action recognition," in *2018 24th International Conference on Pattern Recognition (ICPR)*. IEEE, 2018, pp. 645–650.
- [25] Y. Taigman, M. Yang, M. Ranzato, and L. Wolf, "Deepface: Closing the gap to human-level performance in face verification," in *Proceedings of the IEEE Conference on Computer Vision and Pattern Recognition*, 2014, pp. 1701–1708.
- [26] F. Schroff, D. Kalenichenko, and J. Philbin, "Facenet: A unified embedding for face recognition and clustering," in *Proceedings of the IEEE Conference on Computer Vision and Pattern Recognition (CVPR)*, June 2015.
- [27] J. Zhu, W. Zou, and Z. Zhu, "Two-stream gated fusion convnets for action recognition," in *2018 24th International Conference on Pattern Recognition (ICPR)*. IEEE, 2018, pp. 597–602.
- [28] S. Ren, K. He, R. Girshick, and J. Sun, "Faster r-cnn: towards real-time object detection with region proposal networks," in *Proceedings of the Advances in Neural Information Processing Systems*, 2015, pp. 91–99.
- [29] J. Zhu, W. Zou, L. Xu, Y. Hu, Z. Zhu, M. Chang, J. Huang, G. Huang, and D. Du, "Action machine: Rethinking action recognition in trimmed videos," *arXiv preprint arXiv:1812.05770*, 2018.
- [30] J. Zhu, W. Zou, Z. Zhu, and Y. Hu, "Convolutional relation network for skeleton-based action recognition," *Neurocomputing*, 2019.
- [31] C. Wang, H. K. Galoogahi, C.-H. Lin, and S. Lucey, "Deep-ik for efficient adaptive object tracking," in *2018 IEEE International Conference on Robotics and Automation*. IEEE, 2018, pp. 627–634.
- [32] N. Wang and D.-Y. Yeung, "Learning a deep compact image representation for visual tracking," in *Proceedings of the Advances in Neural Information Processing Systems*, 2013, pp. 809–817.
- [33] H. Li, Y. Li, and F. Porikli, "Deeptrack: Learning discriminative feature representations online for robust visual tracking," *IEEE Transactions on Image Processing*, vol. 25, no. 4, pp. 1834–1848, 2016.
- [34] M. Danelljan, G. Hager, F. S. Khan, and M. Felsberg, "Convolutional features for correlation filter based visual tracking," in *Proceedings*

- of the *IEEE International Conference on Computer Vision Workshop*, 2015, pp. 621–629.
- [35] C. Ma, J.-B. Huang, X. Yang, and M.-H. Yang, “Hierarchical convolutional features for visual tracking,” in *Proceedings of the IEEE International Conference on Computer Vision*, December 2015.
- [36] Y. Qi, S. Zhang, L. Qin, H. Yao, Q. Huang, J. Lim, and M.-H. Yang, “Hedged deep tracking,” in *Proceedings of the IEEE Conference on Computer Vision and Pattern Recognition*, June 2016.
- [37] Y. Song, C. Ma, X. Wu, L. Gong, L. Bao, W. Zuo, C. Shen, L. Rynson, and M.-H. Yang, “Vital: Visual tracking via adversarial learning,” in *Proceedings of the IEEE Conference on Computer Vision and Pattern Recognition*, 2018.
- [38] J. Valmadre, L. Bertinetto, J. F. Henriques, A. Vedaldi, and P. H. S. Torr, “End-to-end representation learning for correlation filter based tracking,” in *Proceedings of the IEEE Conference on Computer Vision and Pattern Recognition*, 2017.
- [39] Y. Song, C. Ma, L. Gong, J. Zhang, R. Lau, and M. H. Yang, “Crest: Convolutional residual learning for visual tracking,” in *Proceedings of the IEEE International Conference on Computer Vision*, 2017.
- [40] H. Fan and H. Ling, “Parallel tracking and verifying: A framework for real-time and high accuracy visual tracking,” in *Proceedings of the IEEE International Conference on Computer Vision*, 2017.
- [41] H. Nam and B. Han, “Learning multi-domain convolutional neural networks for visual tracking,” in *Proceedings of the IEEE Conference on Computer Vision and Pattern Recognition*, June 2016.
- [42] M. Danelljan, A. Robinson, F. S. Khan, and M. Felsberg, “Beyond correlation filters: Learning continuous convolution operators for visual tracking,” in *Proceedings of the European Conference on Computer Vision*, 2016, pp. 472–488.
- [43] M. Danelljan, G. Bhat, F. Shahbaz Khan, and M. Felsberg, “Eco: Efficient convolution operators for tracking,” in *Proceedings of the IEEE Conference on Computer Vision and Pattern Recognition*, July 2017.
- [44] Z. Zhu, W. Wu, W. Zou, and J. Yan, “End-to-end flow correlation tracking with spatial-temporal attention,” in *Proceedings of the IEEE Conference on Computer Vision and Pattern Recognition*. IEEE, 2018.
- [45] Z. Zhu, G. Huang, W. Zou, D. Du, and C. Huang, “Uct: Learning unified convolutional networks for real-time visual tracking,” in *Proceedings of the IEEE International Conference on Computer Vision Workshops*, Oct 2017.
- [46] L. Bertinetto, J. Valmadre, J. F. Henriques, A. Vedaldi, and P. H. S. Torr, “Fully-convolutional siamese networks for object tracking,” in *Proceedings of the European Conference on Computer Vision Workshop*, 2016, pp. 850–865.
- [47] B. Li, W. Wu, Z. Zhu, and J. Yan, “High performance visual tracking with siamese region proposal network,” in *Proceedings of the IEEE Conference on Computer Vision and Pattern Recognition*, 2018.
- [48] Z. Zhu, Q. Wang, B. Li, W. Wu, J. Yan, and W. Hu, “Distractor-aware siamese networks for visual object tracking,” in *Proceedings of the European Conference on Computer Vision (ECCV)*, 2018, pp. 101–117.
- [49] S. Bai, Z. He, T.-B. Xu, Z. Zhu, Y. Dong, and H. Bai, “Multi-hierarchical independent correlation filters for visual tracking,” *arXiv preprint arXiv:1811.10302*, 2018.
- [50] J. Huang, W. Zou, J. Zhu, and Z. Zhu, “Optical flow based real-time moving object detection in unconstrained scenes,” *arXiv preprint arXiv:1807.04890*, 2018.
- [51] J. Huang, W. Zou, Z. Zhu, and J. Zhu, “An efficient optical flow based motion detection method for non-stationary scenes,” *arXiv preprint arXiv:1811.08290*, 2018.
- [52] J. Razlaw, J. Quenzel, and S. Behnke, “Detection and tracking of small objects in sparse 3d laser range data,” in *2019 International Conference on Robotics and Automation*. IEEE, 2019.
- [53] A. V. Gulalkari, G. Hoang, P. S. Pratama, H. K. Kim, S. B. Kim, and B. H. Jun, “Object following control of six-legged robot using kinect camera,” in *International Conference on Advances in Computing, Communications and Informatics*. IEEE, 2014, pp. 758–764.
- [54] Z. Zhu, W. Zou, Q. Wang, and F. Zhang, “Std: A stereo tracking dataset for evaluating binocular tracking algorithms,” in *2016 IEEE International Conference on Robotics and Biomimetics (ROBIO)*. IEEE, 2016, pp. 2215–2220.
- [55] A. V. Gulalkari, P. S. Pratama, G. Hoang, D. H. Kim, B. H. Jun, and S. B. Kim, “Object tracking and following six-legged robot system using kinect camera based on kalman filter and backstepping controller,” *Journal of Mechanical Science and Technology*, vol. 29, no. 12, pp. 5425–5436, 2015.
- [56] A. Mohamed, C. Yang, and A. Cangelosi, “Stereo vision based object tracking control for a movable robot head,” *IFAC-PapersOnLine*, vol. 49, no. 5, pp. 155–162, 2016.
- [57] M. Gupta, S. Kumar, L. Behera, and V. K. Subramanian, “A novel vision-based tracking algorithm for a human-following mobile robot,” *IEEE Transactions on Systems, Man, and Cybernetics: Systems*, vol. 47, no. 7, pp. 1415–1427, 2017.
- [58] Z. Zhu, W. Zou, Q. Wang, and F. Zhang, “A velocity compensation visual servo method for oculomotor control of bionic eyes,” *International Journal of Robotics and Automation*, vol. 33, no. 1, 2018.
- [59] M. Kobilarov, G. Sukhatme, J. Hyams, and P. Batavia, “People tracking and following with mobile robot using an omnidirectional camera and a laser,” in *IEEE International Conference on Robotics and Automation*. IEEE, 2006, pp. 557–562.
- [60] M. Wang, Y. Liu, D. Su, Y. Liao, L. Shi, and J. Xu, “Accurate and real-time 3d tracking for the following robots by fusing vision and ultra-sonar information,” *IEEE/ASME Transactions on Mechatronics*, 2018.
- [61] J. Redmon, S. Divvala, R. Girshick, and A. Farhadi, “You only look once: Unified, real-time object detection,” in *Proceedings of the IEEE conference on computer vision and pattern recognition*, 2016, pp. 779–788.
- [62] A. Dosovitskiy, P. Fischer, E. Ilg, P. Hausser, C. Hazirbas, V. Golkov, P. van der Smagt, D. Cremers, and T. Brox, “Flownet: Learning optical flow with convolutional networks,” in *Proceedings of the IEEE International Conference on Computer Vision*, 2015, pp. 2758–2766.
- [63] R. Tao, E. Gavves, and A. W. M. Smeulders, “Siamese instance search for tracking,” in *Proceedings of the IEEE Conference on Computer Vision and Pattern Recognition*, 2016, pp. 1420–1429.
- [64] D. Held, S. Thrun, and S. Savarese, “Learning to track at 100 fps with deep regression networks,” in *Proceedings of the European Conference on Computer Vision*, 2016, pp. 749–765.